SIAM J. SCI. COMPUT.
Vol. 33, No. 5, pp. 2356–2381

A WELL-BALANCED SYMPLECTICITY-PRESERVING GAS-KINETIC SCHEME FOR HYDRODYNAMIC EQUATIONS UNDER GRAVITATIONAL FIELD*

JUN LUO†, KUN XU†, AND NA LIU‡

Abstract. A well-balanced scheme for an isolated gravitational hydrodynamic system is defined as a scheme which exactly preserves an isothermal hydrostatic solution. In this paper, a well-balanced gas-kinetic symplecticity-preserving BGK (SP-BGK) scheme is developed. In the construction of the scheme, the gravitational potential is modeled as a piecewise constant function inside each cell with a potential jump at the cell interface. In the process of designing such a scheme, the energy conservation, Liouville's theorem, and the symplecticity-preserving property of a Hamiltonian flow play important roles in the description of particles penetration and reflection from a potential barrier. More importantly, the use of the symplecticity-preserving property is crucial in the evaluation of the moments of a postinteraction gas distribution function with a potential jump in terms of the moments of preinteraction distribution function. The SP-BGK method is the first well-balanced shock-capturing gas-kinetic scheme for the Navier–Stokes equation. A few theorems are proved for this scheme, which include the necessity to use an exact Maxwellian for keeping the isothermal hydrostatic state, the total mass and energy (the sum of kinetic, thermal, and gravitational ones) conservation, and the well-balanced property of the SP-BGK scheme to keep an isothermal hydrostatic state during the process of particle transport and collision. Many numerical examples are presented to validate the SP-BGK scheme.

Key words. gas-kinetic scheme, hydrodynamic equations, gravitational potential, symplecticity preserving, well-balanced scheme

AMS subject classifications. 15A15, 15A09, 15A23

DOI. 10.1137/100803699

1. Introduction.

Generally, macroscopic flow equations with source terms can be written as

$$\vec{U}_t + \nabla \cdot F(\vec{U}) = S, \tag{1}$$

where $\vec{U}$ is the vector of conservative flow variables with corresponding fluxes $F(\vec{U})$, and S is the source term. There is an intrinsic steady state solution due to the balance between the flux gradient and source term of equations (1), i.e.,

$$\nabla \cdot F(\vec{U}) = S. \tag{2}$$

The above steady state solution depends on the expression and the boundary condition of the system. The scheme which could keep the above steady state solution may not be a well-balanced scheme, because a well-balanced scheme should be one which drives an isolated gravitational system to an isothermal hydrostatic solution and keeps the

*Submitted to the journal's Computational Methods in Science and Engineering section July 27, 2010; accepted for publication (in revised form) July 12, 2011; published electronically September 27, 2011. This work was supported by Hong Kong Research Grant Council 621709 and RPC10SC11, the National Natural Science Foundation of China (project 10928205), and the National Key Basic Research Program (2009CB724101).

http://www.siam.org/journals/sisc/33-5/80369.html

†Mathematics Department, Hong Kong University of Science and Technology, Clear Water Bay, Kowloon, Hong Kong (maluojun@ust.hk, makxu@ust.hk).

‡LSEC, ICMSEC, Academy of Mathematics and Systems Science, Chinese Academy of Sciences, Beijing 100190, People's Republic of China (liuna@lsec.cc.ac.cn).

solution forever. The designing principle of a well-balanced scheme is not to impose condition (2) directly. It should be an accurate unsteady state flow solver, but it settles the system down to the isothermal hydrostatic solution. For an isolated gravitational system, the only hydrostatic solution should be an isothermal one, which can be explained microscopically. The distribution function of an isolated system under a gravitational field will finally become a steady equilibrium one. Since the collision term will not affect the equilibrium state, the Boltzmann equation goes to

$$\vec{u} \cdot \nabla f - \nabla \phi \cdot \nabla_{\vec{u}} f = 0, \tag{3}$$

where f is the gas distribution function, $\vec{u}$ is the particle velocity, ϕ is the external gravitational potential, and ∇f and $\nabla_{\vec{u}} f$ are the gradients of f with respect to $\vec{x}$ and $\vec{u}$, respectively. The general solution of (3) is

$$f(\vec{x}, \vec{u}) = \mathcal{F}\left(\phi + \frac{1}{2}\vec{u}^2\right), \tag{4}$$

where $\mathcal{F}$ is an arbitrary function and $\vec{u}^2$ is the square of the magnitude of $\vec{u}$. This equilibrium solution clearly shows that the gas of the whole system has the same temperature, because the temperature becomes a constant multiplier for the function $\phi + \frac{1}{2}\vec{u}^2$.

Macroscopically, it may directly use (2) to judge a scheme to be a well-balanced one or not. However, for the gas dynamic equations, this condition is not sufficient. A well-known steady state solution from (2) is the solution with the barotropic equation of state $p = p(\rho)$. For example, the barotropic equation is used to construct a stellar interior solution all the time. However, a scheme with the capability to keep the barotropic solution may not be a well-balanced scheme. The barotropic relation used inside a stellar interior is an approximation. The benefit of this simplification is the absence of the energy equation. In order to sustain the barotropic relationship, the energy cannot be conserved at all, so that there needs to be a continuous energy supply from the solar nuclear energy with convection. But a well-balanced scheme relates to capturing the solution of an isolated system with the full consideration of mass, momentum, and energy. If any fluid element in an isolated system undergoes motion with a barotropic relationship, such as an adiabatic expansion or contraction with $p = C\rho^\gamma$, the fluid element will have a different temperature (due to $p = \rho RT$) from the surrounding gas in the new position. As a result, heat conduction takes effect. According to the second law of thermodynamics, the entropy increases inside an isolated system due to heat conduction, and the system will eventually evolve into an isothermal solution with the maximum amount of entropy for the system. Therefore, for an isolated system the isothermal solution is the only solution which can exist forever.

In order to capture the physical solution of a slowly evolving gravitational hydrodynamic system, the numerical scheme needs to be an accurate shock-capturing scheme as well for the description of general time-dependent gas evolution, and to have a well-balanced property. A well-balanced scheme requires a precise balance between the transport and gravitational source effect in the Boltzmann equation. It is certainly true that the schemes in [5, 14, 2] are well-balanced ones. But the successes in these schemes are mainly based on the reconstruction technique, where the well-balanced solution is directly used from the starting point in order to explicitly enforce the balance (2) of the Euler equations with gravitational source term even in nonhydrostatic situations. For an arbitrary initial condition for an isolated gravitational system, these schemes cannot capture the accurate time evolution of the

system and settle the system to a final correct hydrostatic isothermal solution. For a time-dependent solution, (2) cannot be satisfied and used directly. In [6, 3], the well-balanced property of Roe scheme is imposed through the connection between discontinuous states. For some hydrodynamic equations, e.g., the Navier–Stokes (NS) equations, it is very hard to find such a path to connect two different states. By using the approximate path, these schemes cannot be exactly well balanced.

In the past few years, a gas-kinetic BGK scheme has been successfully developed for compressible Euler and Navier–Stokes equations without gravitational field [11, 12]. The main part of the BGK scheme is to find a gas distribution function f at a cell interface. Physically, the gravitational forcing effect will change the particle trajectory. Theoretically, it shouldn't be difficult for the gas-kinetic scheme to include the gravitational effect in the modification of the time evolution of a gas distribution function through the particle acceleration and deceleration. Along this line, a gas-kinetic scheme for a gravitational system was developed in [10]. This scheme much improves the solution in comparison with the operator splitting method. However, mathematically, the use of a piecewise linear gravitational potential inside each cell makes the exact solution complicated, and a simplification of the particle trajectory in [10] makes the scheme different from a well-balanced one. So, the novelty of this paper is to design a well-balanced scheme with the consideration of particle transport and collision across a potential barrier for hydrodynamic equations under a piecewise constant gravitational potential field. At the same time, the new scheme should still be accurate in capturing any time-dependent gas evolution solution. Dynamically, in a well-balanced situation, the balance between the transport and external forcing effect in the particle movement is very delicate. As shown in this paper, the use of an exact Maxwellian distribution function becomes necessary in designing such a scheme. Also, the use of the symplecticity property of a Hamiltonian flow and Liouville's theorem are important in the correct description of particle penetration, reflection, and deformation across a potential barrier. In a previous paper [13], following the approach of Perthame and Simeoni for the shallow water equations [7], a well-balanced kinetic flux vector-splitting scheme for gravitational Euler equations was developed. However, in [13], only a few low-order moments of a gas distribution function are needed, and these moments can be intuitively guessed. In order to extend the above scheme to high-order accuracy and to solve the NS equations, much more high-order moments of a gas distribution function have to be evaluated for a postinteraction gas distribution function with a potential barrier. In order to systematically evaluate their moments, the use of the symplecticity property of a Hamiltonian particle system is necessary.

The paper is organized as follows. Section 2 gives a brief review of a previous BGK scheme without external forcing field. In section 3, the basic physical principles about the particle interaction with a potential barrier are presented. Section 4 shows the construction of a symplecticity-preserving BGK (SP-BGK) scheme for the gravitational gas dynamic system using the particle transport mechanism derived in the previous section. Section 5 is about the theoretical analysis of the schemes, such as the necessity of using an exact Maxwellian and the well-balanced property. Section 6 shows the numerical tests. The last section is the conclusion.

2. A review of the gas-kinetic BGK-NS scheme without external forcing field. The BGK equation (see [1]) without external forcing field in two dimensions is

$$f_t + \vec{u} \cdot \nabla f = \frac{g - f}{\tau}, \tag{5}$$

where f is the gas distribution function and g is the equilibrium state approached by f, ∇f is the gradient of f with respect to $\vec{x}$, $\vec{x} = (x, y)$, and $\vec{u} = (u, v)$ is the particle velocity. The particle collision time τ is related to the viscosity and heat conduction coefficients, i.e., $\tau = \mu/p$, where μ is the dynamic viscosity coefficient and p is the pressure. The relation between the macroscopic quantities, mass density ρ, momentum density (ρU, ρV), energy density ρE, and the distribution function f is

$$W = \iiint \psi f \mathrm{d}u\mathrm{d}v\mathrm{d}\xi, \tag{6}$$

where $W = (\rho, \rho U, \rho V, \rho E)^T$, (U, V) is the macroscopic velocity of the fluid,

$$\psi = (\psi_1, \psi_2, \psi_3, \psi_4)^T = \left(1, u, v, \frac{1}{2}(u^2 + v^2 + \xi^2)\right)^T,$$

$d\xi = d\xi_1 d\xi_2 ... d\xi_K$, and K is the number of degrees of internal freedom, i.e., $K = (4 - 2\gamma)/(\gamma - 1)$ for two-dimensional (2-D) flow and γ is the specific heat ratio. Since mass, momentum, and energy are conserved during particle collisions, f and g satisfy the conservation constraint,

$$\iiint (g - f)\psi_\alpha \mathrm{d}u\mathrm{d}v\mathrm{d}\xi = 0, \qquad \alpha = 1, 2, 3, 4, \tag{7}$$

at any point in space and time. The integral solution of (5) is

$$f(\vec{x}, t, \vec{u}, \xi) = \frac{1}{\tau}\int_0^t g(\vec{x'}, t', \vec{u}, \xi) e^{-(t-t')/\tau} dt' + e^{-t/\tau} f_0(\vec{x} - \vec{u}t, \vec{u}, \xi), \tag{8}$$

where $\vec{x'} = \vec{x} - \vec{u}(t - t')$ is the particle trajectory. The solution f in (8) solely depends on the modeling of f_0 and g.

For a finite volume scheme, the fluxes across a cell interface need to be evaluated in order to update the cell-average conservative flow variables. In the BGK scheme, the fluxes are defined by

$$F = \iiint u\psi f \mathrm{d}u\mathrm{d}v\mathrm{d}\xi, \tag{9}$$

where $F = (F_\rho, F_{\rho U}, F_{\rho V}, F_{\rho E})^T$, which depends on the gas distribution function f in (8) at the cell interface. Locally, around the cell interface, $\vec{x}_{j+1/2} = (x_{j+1/2}, y_i)$, with the assumption that the x-direction is the normal direction and the y-direction is the tangential direction, a solution in this local coordinate can be obtained.

By using the MUSCL-type limiter, a discontinuous reconstruction of the macroscopic flow variables can be obtained around the cell interface (see Figure 1). The initial gas distribution function f_0 in (8) on both sides of a cell interface can be constructed as

$$\begin{aligned} f_0^l(\vec{x}, \vec{u}, \xi) &= g_0^l(1 + a^l(x - x_{j+1/2}) + b^l(y - y_i) - \tau(a^l u + b^l v + A^l)),\ x \le x_{j+1/2}, \\ f_0^r(\vec{x}, \vec{u}, \xi) &= g_0^r(1 + a^r(x - x_{j+1/2}) + b^r(y - y_i) - \tau(a^r u + b^r v + A^r)),\ x > x_{j+1/2}, \end{aligned} \tag{10}$$

where the Chapman–Enskog expansion up to the NS order has been used in the above initial reconstruction. Here g_0^l and g_0^r are the corresponding Maxwellians

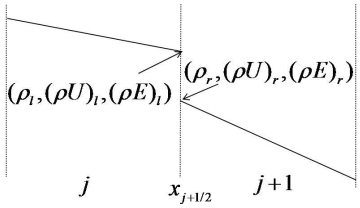

FIG. 1. *Reconstruction of the conservative variables at the cell interface.*

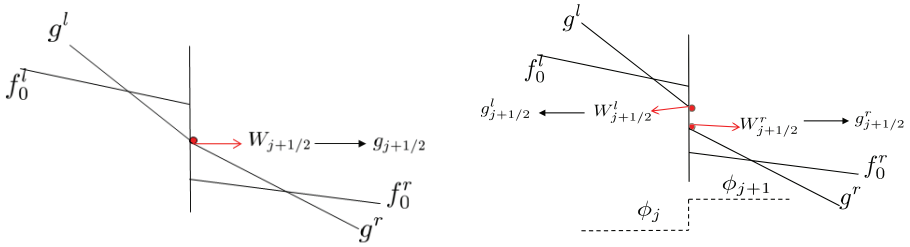

FIG. 2. *The modeling of the initial and equilibrium distribution functions around the cell interface for the BGK scheme without gravity (left) and the SP-BGK scheme with a potential jump (right).*

to $W^l = (\rho_l, (\rho U)_l, (\rho V)_l, (\rho E)_l)^T$ and $W^r = (\rho_r, (\rho U)_r, (\rho V)_r, (\rho E)_r)^T$ on both sides of the interface. The Maxwellian distribution function corresponding to $W = (\rho, (\rho U), (\rho V), (\rho E))^T$ has the form

$$g = \rho \left(\frac{\lambda}{\pi}\right)^{\frac{K+2}{2}} e^{\lambda((u-U)^2+(v-V)^2+\xi^2)}, \tag{11}$$

where λ is equal to $m/2kT$, m is the molecular mass, k is the Boltzmann constant, and T is the temperature. The equilibrium distribution functions around the cell interface can be modeled as

$$\begin{aligned} g^l(\vec{x},t,\vec{u},\xi) &= g^l_{j+1/2}(1+\overline{a}^l(x-x_{j+1/2})+\overline{b}^l(y-y_i)+\overline{A}^l t), \quad x \le x_{j+1/2}, \\ g^r(\vec{x},t,\vec{u},\xi) &= g^r_{j+1/2}(1+\overline{a}^r(x-x_{j+1/2})+\overline{b}^r(y-y_i)+\overline{A}^r t), \quad x > x_{j+1/2}. \end{aligned} \tag{12}$$

In the case without external forcing term, $g^l_{j+1/2}$ and $g^r_{j+1/2}$ in the above equation are the same, i.e., $g^l_{j+1/2} = g^r_{j+1/2}$ (see Figure 2), which can be obtained using the conservation constraint (7) at $\vec{x} = \vec{x}_{j+1/2}$ and $t \to 0$,

$$\begin{aligned} &\iiint g^l_{j+1/2}\psi \mathrm{d}u\mathrm{d}v\mathrm{d}\xi = \iiint g^r_{j+1/2}\psi \mathrm{d}u\mathrm{d}v\mathrm{d}\xi = W_{j+1/2} \\ &= \iiint_{u>0} f_0^l(\vec{x}_{j+1/2},\vec{u},\xi)\psi \mathrm{d}u\mathrm{d}v\mathrm{d}\xi + \iiint_{u<0} f_0^r(\vec{x}_{j+1/2},\vec{u},\xi)\psi \mathrm{d}u\mathrm{d}v\mathrm{d}\xi. \end{aligned} \tag{13}$$

Therefore, at the cell interface the final distribution function can be fully determined

using the integral solution (8). The final distribution function can be written as

$$f(\vec{x}_{j+1/2},t,\vec{u},\xi)=\begin{cases} f^l(\vec{x}_{j+1/2},t,\vec{u},\xi), & u\geq 0,\\ f^r(\vec{x}_{j+1/2},t,\vec{u},\xi), & u<0, \end{cases} \tag{14}$$

where $f^{l,r}(\vec{x}_{j+1/2},t,\vec{u},\xi)$ are the integral solutions in (8) at $(\vec{x}_{j+1/2},t)$ with respect to $g^{l,r}$ and $f_0^{l,r}$. The distribution function (14) is used to evaluate the fluxes

$$\begin{aligned} F^l_{j+1/2}(t)=F^r_{j+1/2}(t)=&\iiint_{u>0} uf^l(\vec{x}_{j+1/2},t,\vec{u},\xi)\psi \mathrm{d}u\mathrm{d}v\mathrm{d}\xi\\ &+\iiint_{u<0} uf^r(\vec{x}_{j+1/2},t,\vec{u},\xi)\psi \mathrm{d}u\mathrm{d}v\mathrm{d}\xi. \end{aligned} \tag{15}$$

The update of the cell-average conservative variables becomes

$$\begin{aligned} W_j^{n+1}=W_j^n+\int_{t_n}^{t_{n+1}}\Big\{&\frac{1}{\Delta x}\left[F^r_{j-1/2}(t)-F^l_{j+1/2}(t)\right]\\ &+\frac{1}{\Delta y}\left[F^r_{i-1/2}(t)-F^l_{i+1/2}(t)\right]\Big\}dt, \end{aligned} \tag{16}$$

where $F^l_{j-1/2}(t)\ \ldots\ F^r_{i+1/2}(t)$ are the fluxes at the center of the cell interfaces.

The definitions and constructions of all parameters related to the spatial and temporal slopes, such as a, b, and A, can be found in [11] and [12].

In summary, at the cell interface $\vec{x}_{j+1/2}$ we can construct the equilibrium distribution functions $g^l_{j+1/2}$ and $g^r_{j+1/2}$ from initial distribution f^l_0 and f^r_0. Also, we can find fluxes $F^l_{j+1/2}(t)$ and $F^r_{j+1/2}(t)$ from the integral solution f^l and f^r. Without an external forcing field, all the particles running into the cell interface can freely cross it. Therefore, the equilibrium states and fluxes at the interface have unique values, i.e., $g^l_{j+1/2}=g^r_{j+1/2}$ and $F^l_{j+1/2}(t)=F^r_{j+1/2}(t)$ (see Figure 2 (left)). In the next section, we will discuss how the potential jump affects the transport of the particles at the cell interface, such as the penetration and reflection from a potential barrier. As a result, the potential jump at the cell interface imposes $g^l_{j+1/2}\neq g^r_{j+1/2}$ (see Figure 2 (right)) and correspondingly $F^l_{j+1/2}(t)\neq F^r_{j+1/2}(t)$.

3. Particle transport mechanism across a potential barrier. In this paper, the gravitational potential ϕ is modeled as a piecewise constant function inside each cell. With ϕ_j in the jth cell and ϕ_{j+1} in the $(j+1)$th cell, there exists a potential jump or barrier at the cell interface. The associated physical impact of the potential jump on a gas distribution function next to it is the reflection or penetration of the particles. For a numerical cell j with $x\in[x_{j-1/2},x_{j+1/2}]$, the fluxes at the two ends of this control volume needs to be evaluated, i.e., $F^r_{j-1/2}(t)$ and $F^l_{j+1/2}(t)$. At any end of a control volume, the particles of the corresponding distribution function are coming from different regions, i.e., the same cell or the neighboring cell after the interaction with a potential jump. Also,the reflection and penetration process happens instantaneously at the interface since the distribution function is defined adjacent the potential barrier. Therefore, once a time-dependent gas distribution function next to the potential barrier is given, the postinteraction distribution function with potential barrier effect can be evaluated simultaneously. The potential barrier affects only

normal velocity of the particles and its moments, so in this section we consider only distribution functions with one-dimensional (1-D) velocity. The results obtained in this section will be used for the construction of the symplecticity-preserving scheme.

For a gas distribution function $f(u)$ next to a potential barrier, the interaction with the potential jump changes the particle velocity from u to u', and the distribution function becomes $\overline{f}(u')$. We use the following three physical principles to find the relation between the velocity moments of $\overline{f}(u')$ and $f(u)$.

(a) *Hamiltonian preserving property:* the Hamiltonian function H of a particle remains constant, i.e.,

$$H = \frac{1}{2}u^2 + \phi(x). \tag{17}$$

This is the energy conservation for a particle movement under a conservative potential field. Since we consider only the interaction of a particle with a potential barrier at an instant of time, there is no collision between particles. Therefore, the energy conservation for individual particle is precisely conserved,

$$\frac{1}{2}u^2 + \phi = \frac{1}{2}(u')^2 + \phi', \tag{18}$$

from which the relation between u and u' can be obtained.

(b) *Liouville's theorem:* the probability density of a particle in phase space keeps a constant along its trajectory,

$$\overline{f}(u') = f(u). \tag{19}$$

In other words, the particle is not lost or created during its impact with the potential barrier.

(c) *The symplecticity-preserving property:* a Hamiltonian phase flow has

$$\iint_{D'} dx'\mathrm{d}u' = \iint_{D} dx\mathrm{d}u, \tag{20}$$

where D' and D are the phase volume of particle movement.

During the impact of the particles with the potential barrier, we specially chose $D = (u_1, u_2) \times (ut_1, ut_2)$; then $D = (u_1', u_2') \times (u't_1, u't_2)$, and (20) changes to

$$\int_{u_1'}^{u_2'} u'\mathrm{d}u' = \int_{u_1}^{u_2} u\mathrm{d}u. \tag{21}$$

This relationship is the most important one to be used in the construction of the connection between moments of $\overline{f}(u')$ and $f(u)$. Therefore, the scheme presented in this paper is called a symplecticity-preserving scheme.

With the above three physical principles, we can derive the relationship between the nth-order velocity moments of $\overline{f}(u')$ and that of $f(u)$. From (19) and (21), we first have

$$\int_{u_1'}^{u_2'} \overline{f}(u')u'\mathrm{d}u' = \int_{u_1}^{u_2} f(u)u\mathrm{d}u. \tag{22}$$

Since (18) gives u' as a function of u, i.e., $u' = u'(u)$, a general formulation can be obtained,

$$n\text{th-order } u \text{ moment} = \int_{u_1'}^{u_2'} \overline{f}(u')(u')^n\mathrm{d}u' = \int_{u_1}^{u_2} f(u)(u'(u))^{n-1}u\mathrm{d}u, \tag{23}$$

which connects the moments of the distribution functions before and after impacting with a potential barrier at an instant of time.

4. The symplecticity-preserving BGK (SP-BGK) scheme.

4.1. The gas-kinetic SP-BGK scheme. With the adaptation of piecewise constant gravitational potential inside each cell, i.e., ϕ_j inside the jth cell, there is a potential jump at the cell interface $\vec{x}_{j+1/2}$. The distribution function f still satisfies (5) inside each cell due to the constant potential. Therefore, a similar framework used in the construction of the BGK-NS scheme can be extended here to design the symplecticity-preserving BGK (SP-BGK) scheme. The initial distribution function is the same as (10). After getting the equilibrium states from the initial distribution function, the integral solution (14) is also valid before considering the effect of the potential jump. But now we need to modify the distribution functions (10) and (14) in order to implement the effect of the potential jump on the equilibrium states construction and the final fluxes evaluation. Due to the potential jump at the cell interface, the construction of equilibrium state at different side of a cell interface needs to take into account all particle collisions from the same cell and from neighboring cells. The particle transport mechanism presented in the last section has to be used to evaluate the moments for the particle from different regions separately.

The potential jump gives a critical speed $U_c = \sqrt{2|\phi_j - \phi_{j+1}|}$, which provides a threshold for the particle movement. Because of the potential jump, not all the particles running into the cell interface could go through it freely. Some may be reflected due to lack of enough kinetic energy to overcome the potential barrier (see Figure 3). For these particles passing through the cell interface, their momentum and energy are changed due to particle acceleration during the transport process.

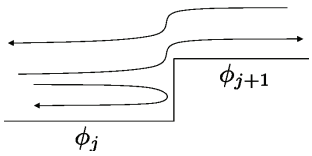

FIG. 3. *The particle's movement at the interface with a potential jump* $\phi_j < \phi_{j+1}$.

Without losing generality, we discuss only the case for $\phi_j < \phi_{j+1}$ in this subsection. Similarly, all the formulae for the case $\phi_j > \phi_{j+1}$ can be obtained. Let's assume a general gas distribution at a cell interface before the interaction with the potential jump is

$$f(\vec{x}_{j+1/2}, t, \vec{u}, \xi) = \begin{cases} f_j(\vec{x}_{j+1/2}, t, \vec{u}, \xi), & u \geq 0, \\ f_{j+1}(\vec{x}_{j+1/2}, t, \vec{u}, \xi), & u < 0. \end{cases} \tag{24}$$

After interaction with the potential jump, the above distribution functions change to $f^l_{j+1/2}(t, \vec{u}, \xi)$ and $f^r_{j+1/2}(t, \vec{u}, \xi)$ on the left- and right-hand sides of the cell interface, respectively,

$$f^l_{j+1/2}(t, \vec{u}, \xi) = \begin{cases} f_j(\vec{x}_{j+1/2}, t, \vec{u}, \xi), & u > 0, \\ \tilde{f}_j(\vec{x}_{j+1/2}, t, \vec{u}, \xi), & 0 \geq u > -U_c, \\ \overline{f}_{j+1}(\vec{x}_{j+1/2}, t, \vec{u}, \xi), & u \leq -U_c, \end{cases} \tag{25}$$

and

$$f^r_{j+1/2}(t,\vec{u},\xi) = \begin{cases} \overline{f}_j(\vec{x}_{j+1/2},t,\vec{u},\xi), & u \geq 0, \\ f_{j+1}(\vec{x}_{j+1/2},t,\vec{u},\xi), & u < 0. \end{cases} \tag{26}$$

The definition of the above distribution functions is from the following consideration (see Figure 3). Because of the potential jump, it affects only the normal particle velocity, u. In (25), $\tilde{f}_j$ is the distribution function of the reflected particle in the jth cell with the original distribution function f_j and positive particle velocity less than U_c. $\overline{f}_{j+1}$ is the distribution function of the particle in the jth cell coming from the $(j+1)$th cell with the original distribution function f_{j+1} and negative particle velocity. The particle has been accelerated in the negative normal direction after passing through the cell interface. Also, $\overline{f}_j$ is the distribution function of the particle in the $(j+1)$th cell coming from the jth cell with the original distribution function f_j and positive particle velocity higher than U_c. The particle gets decelerated in the positive normal direction after passing through the cell interface. Therefore, the effect of the potential jump redistributes the original distribution function on both sides, but the moments of the postinteraction distribution function and the original ones are related through the physical principles introduced in section 3.

Due to the gravitational jump, the main difference between the SP-BGK and BGK-NS schemes is the evaluation of the equilibrium states on both sides of a cell interface, where the corresponding macroscopic variables have to be evaluated based on the moments of distribution functions, which come from different regions. First, the initial gas distribution function f_0, i.e., $f_j(\vec{x}_{j+1/2},t,\vec{u},\xi) = f^l_0(\vec{x}_{j+1/2}-\vec{u}t,\vec{u},\xi)$ and $f_{j+1}(\vec{x}_{j+1/2},t,\vec{u},\xi) = f^r_0(\vec{x}_{j+1/2}-\vec{u}t,\vec{u},\xi)$, changes according to (25) and (26), from which two sets of conservative flow variables on different sides of the cell interface can be obtained,

$$\begin{aligned} W^l_{j+1/2} &= \iiint_{-\infty}^{\infty} f^l_{j+1/2}(t=0,\vec{u},\xi)\psi \mathrm{d}u\mathrm{d}v\xi \\ &= \iiint_{0}^{+\infty} f_j(\vec{x}_{j+1/2},t=0,\vec{u},\xi)\psi \mathrm{d}u + \iiint_{-U_c}^{0} \tilde{f}_j(\vec{x}_{j+1/2},t=0,\vec{u},\xi)\psi \mathrm{d}u\mathrm{d}v\mathrm{d}\xi \\ &\quad + \iiint_{-\infty}^{-U_c} \overline{f}_{j+1}(\vec{x}_{j+1/2},t=0,\vec{u},\xi)\psi \mathrm{d}u\mathrm{d}v\mathrm{d}\xi \end{aligned} \tag{27}$$

and

$$\begin{aligned} W^r_{j+1/2} &= \iiint_{-\infty}^{\infty} f^r_{j+1/2}(t=0,\vec{u},\xi)\psi \mathrm{d}u\mathrm{d}v\xi \\ &= \iiint_{0}^{+\infty} \overline{f}_j(\vec{x}_{j+1/2},t=0,\vec{u},\xi)\psi \mathrm{d}u\mathrm{d}v\mathrm{d}\xi + \iiint_{-\infty}^{0} f_{j+1}(\vec{x}_{j+1/2},t=0,\vec{u},\xi)\psi \mathrm{d}u\mathrm{d}v\mathrm{d}\xi, \end{aligned} \tag{28}$$

from which two Maxwellians $g^l_{j+1/2}$ and $g^r_{j+1/2}$ in the equilibrium states (12) can be fully determined. Then, following the method used in the development of the BGK-NS scheme [12], the integral gas distributions on the left- and right-hand sides of a cell interface, i.e., f^l and f^r in (14), can be obtained. Then, choosing the integral solutions

as the original distribution functions, i.e., $f_j(\vec{x}_{j+1/2},t,\vec{u},\xi) = f^l(\vec{x}_{j+1/2},t,\vec{u},\xi)$ and $f_{j+1}(\vec{x}_{j+1/2},t,\vec{u},\xi) = f^r(\vec{x}_{j+1/2},t,\vec{u},\xi)$, and considering their interactions with the potential jump, these distribution functions are modified according to (25) and (26), from which the corresponding fluxes at different sides of the cell interface can be determined:

(29)
$$\begin{aligned} F^l_{j+1/2}(t) &= \iiint_{-\infty}^{+\infty} u f^l_{j+1/2}(t,\vec{u},\xi)\psi \mathrm{d}u\mathrm{d}v\mathrm{d}\xi \\ &= \iiint_{0}^{+\infty} u f_j(\vec{x}_{j+1/2},t,\vec{u},\xi)\psi \mathrm{d}u + \iint_{-U_c}^{0} u\tilde{f}_j(\vec{x}_{j+1/2},t,\vec{u},\xi)\psi \mathrm{d}u\mathrm{d}v\mathrm{d}\xi \\ &\quad + \iiint_{-\infty}^{-U_c} u\overline{f}_{j+1}(\vec{x}_{j+1/2},t,\vec{u},\xi)\psi \mathrm{d}u\mathrm{d}v\mathrm{d}\xi \end{aligned}$$

and

(30)
$$\begin{aligned} F^r_{j+1/2}(t) &= \iiint_{-\infty}^{+\infty} u f^r_{j+1/2}(t,\vec{u},\xi)\psi \mathrm{d}u\mathrm{d}v\mathrm{d}\xi \\ &= \iiint_{0}^{+\infty} u\overline{f}_j(\vec{x}_{j+1/2},t,\vec{u},\xi)\psi \mathrm{d}u\mathrm{d}v\mathrm{d}\xi + \iiint_{-\infty}^{0} u f_{j+1}(\vec{x}_{j+1/2},t,\vec{u},\xi)\psi \mathrm{d}u\mathrm{d}v\mathrm{d}\xi. \end{aligned}$$

In general, $g^l_{j+1/2} \neq g^r_{j+1/2}$ and $F^l_{j+1/2} \neq F^r_{j+1/2}$. Finally, we can use (16) to update the cell-average conservative variables.

In the above formulae (27), (28), (29), and (30), we need to find the nth-order velocity moments of the modified distribution functions, $\tilde{f}_j$, $\overline{f}_{j+1}$, and $\overline{f}_j$, in terms of the moments of the original distribution functions f_j, f_{j+1}, and f_j, respectively, by (23).

(a) *The nth-order normal velocity moments of* $\tilde{f}_j$. Recall that $\tilde{f}_j$ is the distribution function of the reflected particle in the jth cell. Assume that the normal particle velocity is u before the reflection, and the distribution of the particle before reflection is $f_j(u)$ with $0 < u < U_c$. After its reflection, its velocity becomes u' and $u' = -u$, and (23) gives

$$\int_{-U_c}^{0} \tilde{f}_j(u')(u')^n \mathrm{d}u' = \int_{U_c}^{0} f_j(u)u(-u)^{n-1}\mathrm{d}u = \int_{0}^{U_c} f_j(u)(-1)^n u^n \mathrm{d}u. \tag{31}$$

(b) *The nth-order normal velocity moments of* $\overline{f}_{j+1}$. $\overline{f}_{j+1}$ is the distribution function of the particle in the jth cell coming from the $(j+1)$th cell. Its distribution function before crossing the potential jump is f_{j+1} with normal velocity $u < 0$. After passing through the interface, the normal velocity changes from u to u', where u and u' are related by the Hamiltonian preserving property, i.e.,

$$\frac{1}{2}u^2 + \phi_{j+1} = \frac{1}{2}(u')^2 + \phi_j.$$

So, with $u' = -\sqrt{u^2 + U_c^2}$, (23) gives

$$\int_{-\infty}^{-U_c} \overline{f}_{j+1}(u')(u')^n \mathrm{d}u' = \int_{-\infty}^{0} f_{j+1}(u)(-1)^{n-1}u(u^2+U_c^2)^{(n-1)/2}\mathrm{d}u. \tag{32}$$

(c) *The nth-order normal velocity moments of* $\overline{f}_j$. $\overline{f}_j$ is the distribution function of the particle in the $(j+1)$th cell coming from the jth cell. Its distribution function before passing through the potential jump is f_j with normal velocity $u > U_c$. After passing through the cell interface, the normal velocity changes to u'. The relation between u and u' is

$$\frac{1}{2}u^2 + \phi_j = \frac{1}{2}(u')^2 + \phi_{j+1}.$$

So, with $u' = \sqrt{(u)^2 - U_c^2}$, (23) becomes

$$\int_0^{+\infty} \overline{f}_j(u')(u')^n \mathrm{d}u = \int_{U_c}^{+\infty} f_j(u)u(u^2 - U_c^2)^{(n-1)/2}\mathrm{d}u. \tag{33}$$

Based on the above moment evaluations, we can explicitly evaluate the formulae for $W^l_{j+1/2}$, $W^r_{j+1/2}$, $F^l_{j+1/2}(t)$, and $F^r_{j+1/2}(t)$ by (27)–(33) for the case $\phi_j < \phi_{j+1}$. The formulae for the case $\phi_j > \phi_{j+1}$ can be found similarly. All the formulae are given in the appendix for the 2-D case.

4.2. Limiting cases.

(a) *The* 1*st-order SP-BGK scheme*. Removing all slope terms in (10) and (12), the SP-BGK scheme becomes a 1st-order scheme. The distribution function in (8) becomes

$$f(\vec{x}_{j+1/2}, t, \vec{u}, \xi) = \begin{cases} (1 - e^{-t/\tau})g^l_{j+1/2} + e^{-t/\tau}g^l_0, & u \geq 0, \\ (1 - e^{-t/\tau})g^r_{j+1/2} + e^{-t/\tau}g^r_0, & u < 0, \end{cases} \tag{34}$$

which is called the 1st-order SP-BGK scheme.

(b) *The SP-KFVS scheme*. When the collision time τ goes to $+\infty$, the distribution function in (14) becomes

(35)

$$f(\vec{x}_{j+1/2}, t, \vec{u}, \xi) = \begin{cases} f^l(\vec{x}_{j+1/2}, t, \vec{u}, \xi), & u \geq 0, \\ f^r(\vec{x}_{j+1/2}, t, \vec{u}, \xi), & u < 0, \end{cases} = \begin{cases} f^l_0(\vec{x}_{j+1/2} - \vec{u}t), & u \geq 0, \\ f^r_0(\vec{x}_{j+1/2} - \vec{u}t), & u < 0. \end{cases}$$

The above solution solely comes from free transport, and there is no contribution of the equilibrium states g in the integral solution f. It is equivalent to solving

$$f_t + \vec{u} \cdot \nabla f = 0$$

directly when the initial distribution function is modeled as (10). In other words, we don't consider particle collision here, and need not model the equilibrium distribution function g in (12). This is exactly the same scheme introduced in [13], which is called the symplecticity-preserving kinetic flux vector splitting (SP-KFVS) scheme. It is actually a limiting case of the SP-BGK scheme.

5. Theoretical analysis. For simplicity, we prove all the theorems in the 1-D case. But all the conclusions still hold for multiple dimensions as well, because the potential jump exists only in the normal direction when we consider a 2-D cell interface. The particle velocity in other directions doesn't affect the dynamical property in

the normal direction. When $V = 0$ in macroscopic velocity $\vec{U} = (U, V)$, the formulae in the appendix become the formulae for the 1-D case.

In the current scheme, the updated flow variables inside each cell are the mass, momentum, and energy densities (kinetic + thermal ones). The gravitational energy is not explicitly included. However, for an isolated gravitational system, the total energy (kinetic + thermal + gravitational ones) conservation is a necessary condition in order to get a correct physical solution. In the following theorem, we are first going to prove the conservation of total energy.

THEOREM 5.1. *The SP-KFVS and SP-BGK schemes are mass and total energy conservative schemes.*

Proof. The only difference between the SP-KFVS and SP-BGK schemes is that they have different original distribution functions $f_j(u)$ and $f_{j+1}(u)$. However, whatever $f_j(u)$ and $f_{j+1}(u)$ are, the mass and total energy are updated according to the fluxes calculated by (70) and (71) or (72) and (73) in the appendix. The concept of conservation of a variable means that the change of that variable in any fixed domain depends only on the fluxes across the interfaces of that control volume. We assume the control volume consists of cells between the cell-index K_1 and K_2, where $K_1 < K_2$. Then by direct calculation, we have the following.

Mass conservation:

$$\sum_{j=K_1}^{K_2} \rho_j^{n+1} = \sum_{j=K_1}^{K_2} \rho_j^n + \frac{1}{\Delta x} \int_{t_n}^{t_{n+1}} \left[F^r_{K_1-1/2,\rho} - F^l_{K_2+1/2,\rho} \right] \mathrm{d}t. \tag{36}$$

Total energy conservation:

$$\begin{aligned} \sum_{j=K_1}^{K_2} TE_j^{n+1} = \sum_{j=K_1}^{K_2} TE_j^n + \frac{1}{\Delta x} \int_{t_n}^{t_{n+1}} \Big[& F^r_{K_1-1/2,\rho}\phi_{K_1} - F^l_{K_2+1/2,\rho}\phi_{K_2} \\ & + F^r_{K_1-1/2,\rho E} - F^l_{K_2+1/2,\rho E} \Big] \mathrm{d}t. \end{aligned} \tag{37}$$

Therefore, the SP-KFVS and SP-BGK schemes can give the correct shock location even with the external gravitational forcing term. This is a generalization of the Lax–Wendroff theorem to the system with gravitational source term [4].

LEMMA 5.2. *The density $\rho(x)$ of an isothermal hydrostatic state under the gravitational field $\phi(x)$ in a gas dynamic system satisfies*

$$\rho(x) = C_1 e^{-2\tilde{\lambda}\phi(x)}, \tag{38}$$

where C_1 and $\tilde{\lambda}$ are constants.

Proof. In the gas dynamic system, an isothermal hydrostatic solution under the gravitational field $\phi(x)$ as mentioned in the introduction satisfies

$$p_x = -\rho\phi_x, \quad T = \text{constant}, \quad U = 0. \tag{39}$$

Since $T =$ constant and $\tilde{\lambda} = m/2kT$, $\tilde{\lambda}$ is also a constant. Then from (39) and the ideal gas equation of state

$$p = \frac{1}{2\tilde{\lambda}}\rho,$$

we have

$$\frac{1}{2\tilde{\lambda}}\rho_x = -\rho\phi_x.$$

Therefore, with a constant C_1, the solution becomes

$$\rho(x) = C_1 e^{-2\tilde{\lambda}\phi(x)}.$$

Remark. For the well-balanced scheme, the hydrostatic solution always means the above isothermal hydrostatic one. Without losing generality, in the following proofs, we always let $C_1 = 1$ for the hydrostatic solution. So, in the hydrostatic case, the state has the form

$$\rho = e^{-2\tilde{\lambda}\phi(x)}, \quad U = 0, \tag{40}$$

where $\tilde{\lambda}$ is a constant. Numerically, if we let the potential $\phi(x)$ be a constant, ϕ_j, in the jth cell; then

$$\rho_{j+1} = \rho_j e^{-2\tilde{\lambda}(\phi_{j+1}-\phi_j)}, \quad U_j = 0, \tag{41}$$

where ρ_j and U_j are cell average quantities.

LEMMA 5.3. *The equilibrium state construction depends on the corresponding macroscopic variables* $W^l_{j+1/2} = (\rho^l_{j+1/2}, (\rho U)^l_{j+1/2}, (\rho E)^l_{j+1/2})^T$ *and* $W^r_{j+1/2} = (\rho^r_{j+1/2}, (\rho U)^r_{j+1/2}, (\rho E)^r_{j+1/2})^T$ *obtained from postinteraction distribution functions on the left- and right-hand sides of a cell interface. Starting from an initial hydrostatic state, the above constructed macroscopic variables have the following properties.*

1. *Both velocities are equal to zero, i.e.,*

$$U^l_{j+1/2} = U^r_{j+1/2} = 0. \tag{42}$$

2. *They have the same temperature on both sides of all cell interfaces, i.e.,*

$$\lambda^l_{j+1/2} = \lambda^r_{j+1/2} = \tilde{\lambda}, \tag{43}$$

where $\tilde{\lambda}$ *is the constant of the initial hydrostatic solution.*

3. *The densities at both sides of the same cell interface satisfy*

$$\rho^r_{j+1/2} = \rho^l_{j+1/2} e^{-2\tilde{\lambda}(\phi_{j+1}-\phi_j)}. \tag{44}$$

4. *In the same cell,*

$$\rho^l_{j+1/2} = \rho^r_{j-1/2}. \tag{45}$$

Proof. With the definition $f_j(u) = g_j(u)$ and $g_j(u)$ being a Maxwellian corresponding to the cell-average conservative variables $(\rho_j, (\rho U)_j, (\rho E)_j)$, $W^l_{j+1/2}$ and $W^r_{j+1/2}$ are determined by (66) and (67) or (68) and (69) for $\phi_j < \phi_{j+1}$ or $\phi_j > \phi_{j+1}$. Here, we prove only the case for $\phi_j < \phi_{j+1}$. The other case can be proved similarly. From direct calculation, we can get

$$\begin{aligned} \rho^l_{j+1/2} = \frac{\rho_j}{2} &+ \rho_j \left(\frac{\tilde{\lambda}}{\pi}\right)^{\frac{1}{2}} \int_{-U_c}^{0} e^{-\tilde{\lambda}u^2} \mathrm{d}u \\ &- \rho_{j+1} \left(\frac{\tilde{\lambda}}{\pi}\right)^{\frac{1}{2}} U_c + \rho_{j+1}\tilde{\lambda} \left(\frac{\tilde{\lambda}}{\pi}\right)^{\frac{1}{2}} \int_0^{+\infty} e^{-\tilde{\lambda}t} \sqrt{t + U_c^2} \mathrm{d}t, \end{aligned} \tag{46}$$

$$\rho_{j+1/2}^r = \rho_j \tilde{\lambda} \left(\frac{\tilde{\lambda}}{\pi}\right)^{\frac{1}{2}} \int_{U_c^2}^{+\infty} e^{-\tilde{\lambda}t} \sqrt{t - U_c^2} \mathrm{d}t + \frac{\rho_{j+1}}{2}, \tag{47}$$

$$(\rho U)_{j+1/2}^l = (\rho U)_{j+1/2}^r = 0, \tag{48}$$

$$\begin{aligned}(\rho E)_{j+1/2}^l = {} & \frac{K}{4\tilde{\lambda}} \rho_{j+1/2}^l + \frac{\rho_j}{8\tilde{\lambda}} - \frac{\rho_j}{4\tilde{\lambda}} \sqrt{\frac{\tilde{\lambda}}{\pi}} e^{-\tilde{\lambda} U_c^2} U_c + \frac{\rho_j}{4\tilde{\lambda}} \sqrt{\frac{\tilde{\lambda}}{\pi}} \int_{-U_c}^{0} e^{-\tilde{\lambda} u^2} \mathrm{d}u \\ & + \frac{\rho_{j+1}}{4} \sqrt{\frac{\tilde{\lambda}}{\pi}} \int_0^{+\infty} e^{-\tilde{\lambda} t} \sqrt{t + U_c^2} \mathrm{d}t,\end{aligned} \tag{49}$$

and

$$(\rho E)_{j+1/2}^r = \frac{K}{4\tilde{\lambda}} \rho_{j+1/2}^r + \frac{\rho_j}{4} \sqrt{\frac{\tilde{\lambda}}{\pi}} \int_{U_c^2}^{+\infty} e^{-\tilde{\lambda} t} \sqrt{t - U_c^2} \mathrm{d}t + \frac{\rho_{j+1}}{8\tilde{\lambda}}, \tag{50}$$

where $U_c = \sqrt{2(\phi_{j+1} - \phi_j)}$.

1. From (46) and (47), we can see that $\rho_{j+1/2}^l > 0$ and $\rho_{j+1/2}^r > 0$ when $\rho_j > 0$ and $\rho_{j+1} > 0$. Since $U = \rho U / \rho$, from (48), we get

$$U_{j+1/2}^l = U_{j+1/2}^r = 0.$$

2. Macroscopically, λ satisfies

$$\rho E - \frac{1}{2} \rho U^2 = \rho \frac{K+1}{4\lambda}, \tag{51}$$

where $K = (3 - \gamma)/(\gamma - 1)$ in one dimension. From (46),

$$\begin{aligned}\rho_{j+1/2}^l \frac{K+1}{4\lambda_{j+1/2}^l} = {} & \frac{K}{4\lambda_{j+1/2}^l} \rho_{j+1/2}^l + \frac{\rho_j}{8\lambda_{j+1/2}^l} + \frac{\rho_{j+1}}{4\lambda_{j+1/2}^l} \sqrt{\frac{\tilde{\lambda}}{\pi}} U_c + \frac{\rho_j}{4\lambda_{j+1/2}^l} \sqrt{\frac{\tilde{\lambda}}{\pi}} \int_{-U_c}^{0} e^{-\tilde{\lambda} u^2} \mathrm{d}u \\ & + \frac{\rho_{j+1}}{4\lambda_{j+1/2}^l} \tilde{\lambda} \sqrt{\frac{\tilde{\lambda}}{\pi}} \int_0^{+\infty} e^{-\tilde{\lambda} t} \sqrt{t + U_c^2} \mathrm{d}t.\end{aligned} \tag{52}$$

Since $(\rho E)_{j+1/2}^l - \frac{1}{2} \rho_{j+1/2}^l (U_{j+1/2}^l)^2 = \rho_{j+1/2}^l \frac{K+1}{4\lambda_{j+1/2}^l}$ (see [11]) and $U_{j+1/2}^l = 0$, we have

$$\begin{aligned}(\lambda_{j+1/2}^l - \tilde{\lambda}) \Bigg\{ & \frac{1}{\lambda_{j+1/2}^l \tilde{\lambda}} \left(\frac{K}{4} \rho_{j+1/2}^l + \frac{\rho_j}{8} - \frac{\rho_j}{4} \sqrt{\frac{\tilde{\lambda}}{\pi}} e^{-\tilde{\lambda} U_c^2} U_c \right. \\ & \left. + \frac{\rho_j}{4} \sqrt{\frac{\tilde{\lambda}}{\pi}} \int_{-U_c}^{0} e^{-\tilde{\lambda} u^2} \mathrm{d}u \right) + \frac{1}{\lambda_{j+1/2}^l} \frac{\rho_{j+1}}{4} \sqrt{\frac{\tilde{\lambda}}{\pi}} \int_0^{+\infty} e^{-\tilde{\lambda} t} \sqrt{t + U_c^2} \mathrm{d}t \Bigg\} = 0.\end{aligned} \tag{53}$$

The summation in the braces {...} of (53) is strictly larger than zero. Therefore,

$$\lambda^l_{j+1/2} = \tilde{\lambda}.$$

Similarly, we can prove

$$\lambda^r_{j+1/2} = \tilde{\lambda}.$$

3. It is easy to prove that

$$\int_{-U_c}^{0} e^{-\tilde{\lambda}u^2}\mathrm{d}u = e^{-\lambda U_c^2}U_c + 2\tilde{\lambda}\int_{-U_c}^{0} e^{-\tilde{\lambda}u^2}u^2\mathrm{d}u. \tag{54}$$

So, $\rho^r_{j+1/2} = \rho^l_{j+1/2}e^{-2\tilde{\lambda}(\phi_{j+1}-\phi_j)}$, $\xleftrightarrow{(46),(47),(54)}$ (is equivalent to) $\int_{U_c^2}^{+\infty} e^{-\tilde{\lambda}t}\sqrt{t-U_c^2}\mathrm{d}t = 2e^{-\tilde{\lambda}U_c^2}\int_{-U_c}^{0} e^{-\tilde{\lambda}u^2}u^2\mathrm{d}u + e^{-2\tilde{\lambda}U_c^2}\int_0^{+\infty} e^{-\tilde{\lambda}t}\sqrt{t+U_c^2}\mathrm{d}t$, $\xleftrightarrow{left:x=t-U_c^2;right:x=t+U_c^2}$ $\int_0^{+\infty} e^{-\tilde{\lambda}x}\sqrt{x}\mathrm{d}x = 2\int_{-U_c}^{0} e^{-\tilde{\lambda}u^2}u^2\mathrm{d}u + \int_{U_c^2}^{+\infty} e^{-\tilde{\lambda}x}\sqrt{x}\mathrm{d}x$ $\Longleftrightarrow \int_0^{U_c^2} e^{-\tilde{\lambda}x}\sqrt{x}\mathrm{d}x = 2\int_{-u_c}^{0} e^{-\tilde{\lambda}u^2}u^2\mathrm{d}u$, which is true.

Therefore,

$$\rho^r_{j+1/2} = \rho^l_{j+1/2}e^{-2\tilde{\lambda}(\phi_{j+1}-\phi_j)}.$$

4. $\rho^l_{j+1/2} = \rho^r_{j-1/2}$, $\xleftrightarrow{(46),(47),(41),(54)}$ $2\tilde{\lambda}\rho_j\int_{-U_c}^{0} e^{-\tilde{\lambda}u^2}u^2\mathrm{d}u + \rho_j\tilde{\lambda}\int_{U_c^2}^{+\infty} e^{-\tilde{\lambda}x}\sqrt{x}\mathrm{d}x = \rho_j\tilde{\lambda}\int_0^{+\infty} e^{-\tilde{\lambda}x}\sqrt{x}\mathrm{d}x$, which is also correct. Therefore,

$$\rho^l_{j+1/2} = \rho^r_{j-1/2}.$$

Remark. The above lemma, especially part 2, illustrates that starting from a hydrostatic state with the same temperature, the constructed equilibrium states on both sides of a cell interface have equal temperature as well. In order words, in the hydrostatic case, particle interaction with the potential barrier and particle collisions among themselves never alter the equilibrium temperature on both sides of a cell interface. This is consistent with the second law of thermodynamics. Otherwise, the temperature differences generated by the particle interaction with a potential barrier and the collisions among themselves could be used to design an engine to extract work from an initially isothermal system, which violates the second law of thermodynamics.

THEOREM 5.4. *For a well-balanced kinetic scheme, the equilibrium distribution function must be an "exact Maxwellian."*

Proof. In order to keep the hydrostatic solution (41), the numerical mass flux on both sides of a cell interface must be zero.

Without losing generality, we consider only the case for $\phi_{j+1} > \phi_j$. Since the gas must be isotropic, we can assume the equilibrium distribution function is $\rho(x)G(u^2)$ and define $a = \sqrt{2(\phi_{j+1}-\phi_j)}$. Then we require

$$F^r_{j+1/2,\rho} = \int_a^{+\infty} \rho_j G(u^2)u\mathrm{d}u + \int_{-\infty}^{0} \rho_{j+1}G(u^2)u\mathrm{d}u = 0, \tag{55}$$

where $F^r_{j+1/2,\rho}$ is the mass flux on the right side of the interface. Because of (41), we have

$$\frac{1}{2}\int_{a^2}^{+\infty} G(x)\mathrm{d}x + e^{-\lambda a^2}\int_{-\infty}^{0} G(u^2)u\mathrm{d}u = 0. \tag{56}$$

Taking the derivative of (56) with a^2, we get

$$-\frac{1}{2}G(a^2) - \lambda e^{-\lambda a^2}\int_{-\infty}^{0} G(u^2)u\mathrm{d}u = 0. \tag{57}$$

It is obvious from (57) that

$$G(a^2) \sim e^{-\lambda a^2}, \tag{58}$$

which means that the equilibrium distribution function is an exact Maxwellian distribution.

THEOREM 5.5. *The 1st-order SP-KFVS and SP-BGK schemes are both well-balanced schemes.*

Proof. In order to prove a scheme to be a well-balanced one, we only need to verify that the scheme can keep the hydrostatic solution (40) forever. Numerically, the initial condition for this case is given by (41) in the jth cell. At the next time step, the above solution must be kept by the well-balanced numerical scheme, i.e., $W_j^{n+1} = W_j^n$. From (16), we must have

$$F_{j-1/2}^r = F_{j+1/2}^l. \tag{59}$$

Therefore, to complete the proof, we have to show that mass fluxes ($F_{j+1/2,\rho}^{r,l}$), momentum fluxes ($F_{j+1/2,\rho U}^{r,l}$), and energy fluxes ($F_{j+1/2,\rho E}^{r,l}$) satisfy condition (59), respectively.

The 1st-order SP-KFVS scheme. The original distribution function at the cell interface is

$$f(x_{j+1/2},t,u,\xi) = \begin{cases} g_j(u), & u \geq 0, \\ g_{j+1}(u), & u < 0, \end{cases} \tag{60}$$

where $g_j(u)$ is the Maxwellian corresponding to $(\rho_j, (\rho U)_j, (\rho E)_j)$. The proof is only a direct calculation of the fluxes at the interface using (70) and (71) or (72) and (73) in two different cases for $\phi_j < \phi_{j+1}$ or $\phi_j > \phi_{j+1}$ when the initial hydrostatic condition (41) can be satisfied. The results are the following.

(a) For mass flux,

$$F_{j+1/2,\rho}^l = F_{j-1/2,\rho}^r = 0. \tag{61}$$

(b) For momentum flux,

$$F_{j+1/2,\rho U}^l = F_{j-1/2,\rho U}^r = \frac{\rho_j}{2\lambda}. \tag{62}$$

(c) For energy flux,

$$F_{j+1/2,\rho E}^l = F_{j-1/2,\rho E}^r = 0. \tag{63}$$

Hence, the 1st-order SP-KFVS scheme is a well-balanced one.

The 1st-order SP-BGK scheme. The original distribution function is

$$f(x_{j+1/2},t,u,\xi)=\begin{cases}(1-\epsilon)g_j(u)+\epsilon g^l_{j+1/2}(u), & u\geq 0,\\ (1-\epsilon)g_{j+1}(u)+\epsilon g^r_{j+1/2}(u), & u<0,\end{cases} \tag{64}$$

where ϵ belongs to $(0,1)$ and is independent of u, $g_j(u)$ is the same as that in the proof for the 1st-order SP-KFVS scheme, and $g^l_{j+1/2}$ and $g^r_{j+1/2}$ are two equilibrium states corresponding to $W^l_{j+1/2}$ and $W^r_{j+1/2}$, respectively. Here, $W^l_{j+1/2}$ and $W^r_{j+1/2}$ are the macroscopic variables calculated by (66) and (67) or (68) and (69) when

$$f_j(u)=g_j(u) \text{ and } f_{j+1}(u)=g_{j+1}(u).$$

So, the fluxes are the linear combination of two kinds of fluxes F_1 and F_2 which are calculated by

$$f_1=\begin{cases}g_j(u), & u\geq 0,\\ g_{j+1}(u), & u<0,\end{cases} \text{ and } f_2=\begin{cases}g^l_{j+1/2}(u), & u\geq 0,\\ g^r_{j+1/2}(u), & u<0,\end{cases}$$

respectively.

From the above proof for the 1st-order SP-KFVS scheme, we know that the fluxes F_1 can satisfy (59). Therefore, we only need to prove that F_2 can satisfy (59), too. Note that in the proof for the 1st-order SP-KFVS scheme, the hydrostatic initial condition (41) is the key. From Lemma 5.3, we know that the equilibrium states also satisfy the hydrostatic initial condition. So, we can get the same results for the fluxes corresponding to f_2 based on (61), (62), and (63) with $W^l_{j+1/2}$ and $W^r_{j+1/2}$.

From all the above proofs, we can conclude that the 1st-order SP-KFVS and SP-BGK schemes both can keep the hydrostatic solution forever. Therefore, they are well-balanced schemes.

Remark. In order to make sure the 2nd-order SP-KFVS and SP-BGK schemes are well-balanced schemes, we use $(U,\ \lambda,\ \rho e^{2\lambda\phi})$ to do the reconstruction at the beginning of each time step. Specifically, for a hydrostatic solution, the flow variables satisfy the conditions

$$U=0,\quad V=0,\quad \lambda=\text{constant},\quad Ba=\text{constant}, \tag{65}$$

where $Ba=\rho e^{2\lambda\phi}$. We first apply a MUSCL-type limiter to reconstruct the slopes of $(U,\ V,\ \lambda,\ Ba)$, i.e., $(S_U,\ S_V,\ S_\lambda,\ S_{Ba})$ inside each cell. Since

$$\rho=\frac{Ba}{e^{2\lambda\phi}},\ \rho E=\frac{1}{2}\rho(U^2+V^2)+\frac{K+2}{4\lambda}\rho,$$

we can get the corresponding slopes for other flow variables,

$$S_\rho=\frac{1}{e^{2\lambda\phi}}S_{Ba}-2\rho\phi S_\lambda,\ S_{\rho U}=S_\rho U+\rho S_U,\ S_{\rho V}=S_\rho V+\rho S_V,$$

$$S_{\rho E}=\left[\frac{1}{2}(U^2+V^2)+\frac{K+2}{4\lambda}\right]S_\rho+\rho\left[US_U+VS_V-\frac{K+2}{4\lambda^2}S_\lambda\right],$$

where $(S_\rho,\ S_{\rho U},\ S_{\rho V},\ S_{\rho E})$ are the slopes of $(\rho,\ \rho U,\ \rho V,\ \rho E)$ inside that cell. Therefore, we can reconstruct $(\rho,\ \rho U,\ \rho V,\ \rho E)$ in each cell using its cell-average quantities and the above slopes. Here, all slopes become zeros when the initial flow is in a hydrostatic state, and the reconstruction doesn't introduce numerical error. In other words, the 2nd-order schemes go back to the 1st-order schemes when the solution is in a hydrostatic state. Therefore, the 2nd-order schemes are also well-balanced ones.

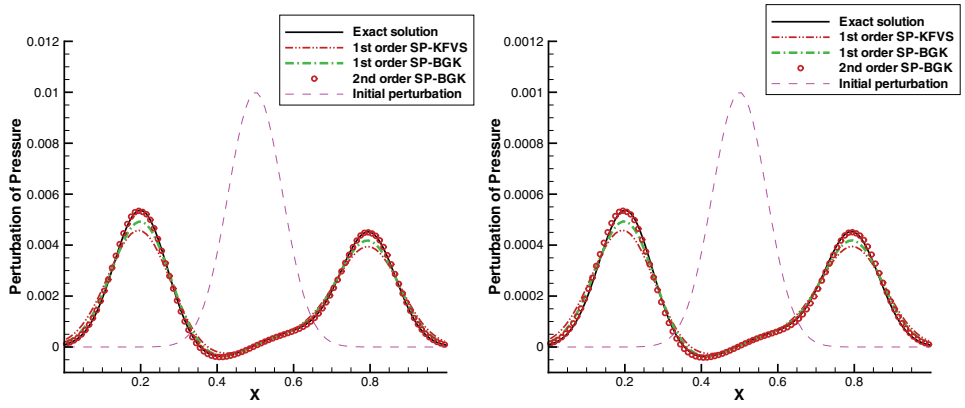

FIG. 4. *Propagation of the pressure perturbation starting from an isothermal equilibrium solution. Left:* $\eta = 0.01$*; right:* $\eta = 0.001$.

6. Numerical examples. In this section, we will present numerical results in both the 1-D and 2-D cases. Each of the examples is very sensitive to the accuracy of the scheme. Some of the tests run for millions of time steps. If the scheme is not a well-balanced one, the accumulation of any small numerical error would become significant for such a long time evolution (see [10]).

6.1. Perturbation of the 1-D isothermal equilibrium solution. This test case is from LeVeque and Bale's paper [5]. An ideal gas with $\gamma = 1.4$ stays initially in an isothermal hydrostatic state,

$$\rho_0(x) = p_0(x) = e^{-x} \quad \text{and} \quad U_0(x) = 0$$

for $x \in [0, 1]$. Then the initial pressure is perturbed by

$$p(x, t = 0) = p_0(x) + \eta e^{\alpha(x-x_0)^2},$$

where $\alpha = 100$, $x_0 = 0.5$, and η is the amplitude of the perturbation. The gravitational force G takes a value $G = -1.0$ in the x-direction. So the potential jump at each cell interface becomes

$$\phi_{j+1} - \phi_j = -G\Delta x = 0.01.$$

The computation is conducted with 100 grid points in the whole domain and stops at time $t = 0.25$. As shown in [5] and [10], an operator splitting scheme can't capture the small perturbation. The gravitational effect has to be explicitly included in the calculation of fluxes. Our schemes give good results, especially for the 2nd-order SP-BGK scheme (see Figure 4). The SP-KFVS scheme has larger numerical dissipation due to its free transport mechanism than the SP-BGK scheme, and the 1st-order scheme is more dissipative than the 2nd-order one.

Figure 5 shows the convergency rate of the 2nd-order SP-BGK scheme, where the number of cells is N and the error is the L^∞ error. From these figures, we can conclude that the 2nd-order SP-BGK scheme has a 2nd-order accuracy even with the modeling of piecewise constant potential.

6.2. Shock tube under gravitational field. This case is the standard Sod test under gravitational field. The computational domain is $x \in [0, 1]$, which is divided

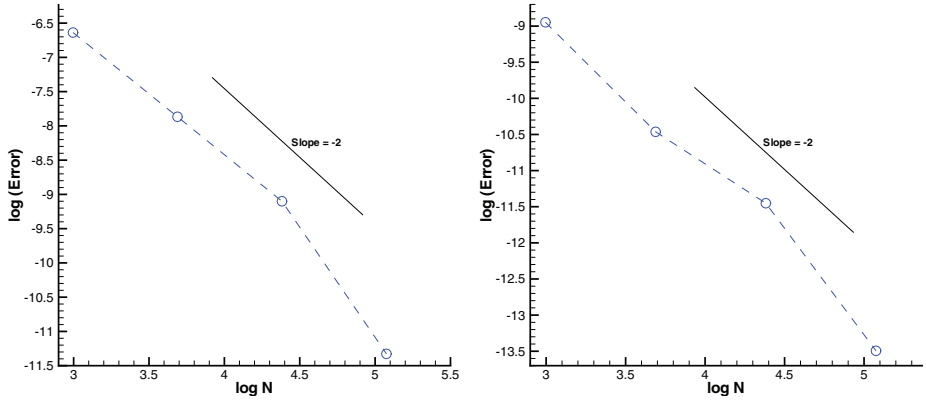

FIG. 5. *Convergency rate of the 2nd-order SP-BGK scheme for the pressure perturbation starting from an isothermal equilibrium solution with* $\eta = 0.01$ *on the left figure, and* $\eta = 0.001$ *on the right figure.*

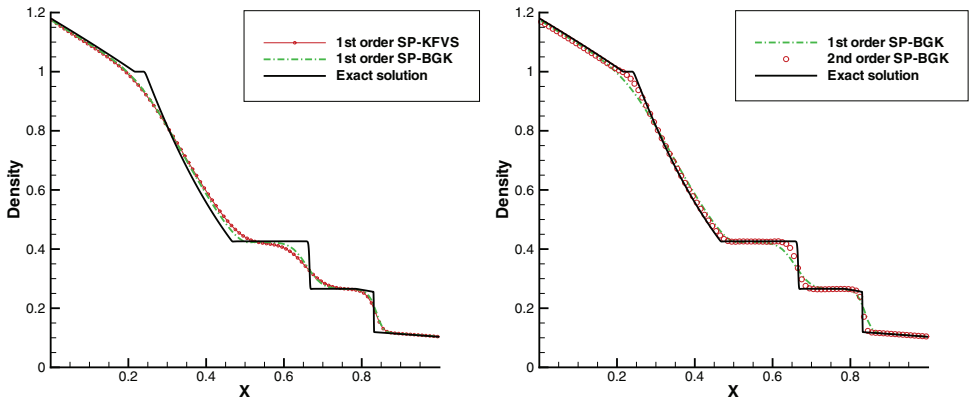

FIG. 6. *Density distributions for the shock tube problem under gravitational field. From the comparison of different schemes, the dissipation of the SP-BGK scheme is much smaller than the SP-KFVS scheme.*

into 100 cells. Adiabatic reflection boundary condition is used on both ends. The initial condition is

$$\rho = 1.0,\ U = 0.0,\ p = 1.0 \text{ for } x \leq 0.5$$

and

$$\rho = 0.125,\ U = 0.0,\ p = 0.1 \text{ for } x > 0.5.$$

The gravitational field is the same as in section 6.1. The computational results at $t = 0.2$ are presented in Figures 6 and 7. Due to the gravitational force, the density distribution inside the tube is pulled back in the negative x-direction. In some region, the flow velocity even becomes negative. This test case illustrates that the SP-BGK scheme has the shock-capturing property. These schemes which explicitly impose the well-balanced condition may lose the shock-capturing property in this case.

6.3. One-dimensional gas falling into a fixed external potential. This case is taken from the paper by Slyz and Prendergast [9] to investigate the numerical

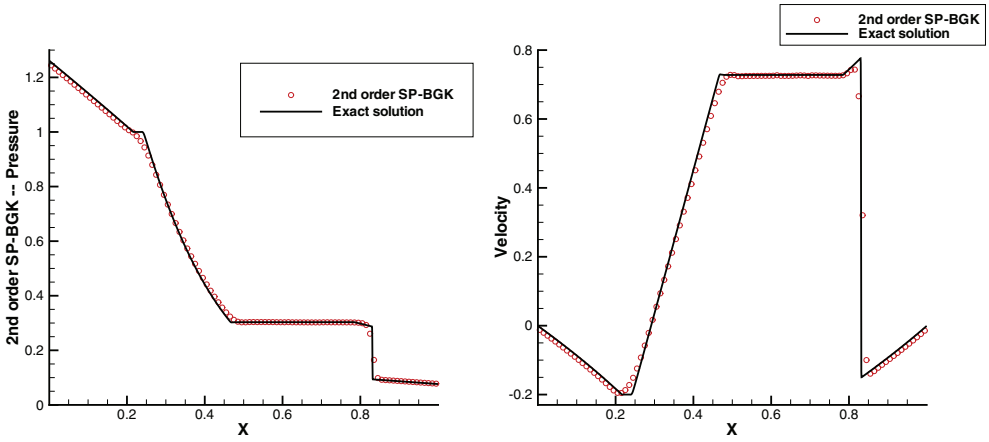

FIG. 7. *Pressure and velocity distributions from the 2nd-order SP-BGK scheme for the shock tube problem under gravitational field. The shock-capturing property of the SP-BGK scheme is clearly shown in this test case.*

accuracy of the BGK scheme. The gas is initially stationary ($U = 0$) and homogeneous ($\rho = 1$, $e = 1$, where e is the internal energy). The gravitational potential has the form of a sine wave,

$$\phi = -\phi_0 \frac{L}{2\pi} \sin \frac{2\pi x}{L},$$

where $L = 64$ is the length of the computational domain and $\phi_0 = 0.02$. The ratio of the specific heat has a value $\gamma = 5/3$. The periodic boundary conditions are implemented in this system. Simulation results are presented with $\Delta x = 1$ and an output time $t = 2500000$ (more than 5000000 time steps). After the initial transition, the system is expected to reach an isothermal hydrostatic state, where the temperature settles to a constant and fluid velocity is zero, i.e.,

$$T(x,t) = T_0 \quad \text{and} \quad U = 0.$$

The velocity and temperature distributions computed by different symplecticity-preserving schemes are shown in Figures 8 and 9. The EST-BGK is the scheme developed in [10]. The velocity distribution shows that the SP-BGK scheme can keep the hydrostatic solution much better than that in [10]. And the error in the SP-BGK scheme is due to the numerical integration of many integrals in (66)–(69) and (70)–(73). For example, $\int_{-\infty}^{0} g(u)(-\frac{u}{\sqrt{u^2+U_c^2}})\mathrm{d}u$ can't be calculated exactly, and the numerical integration has to be used to get the solution. With the reduction of the numerical integration error through the increasing of integration points, the results can be improved. Theoretically, without numerical integration error the SP-BGK and SP-KFVS schemes are well-balanced ones, where the exact hydrostatic solution can be kept forever. However, it is impossible to improve the results in [10] because the EST-BGK scheme is not a well-balanced one due to the simplification of particle trajectory in a linearly distributed potential field. In these figures, the results are calculated by the 2nd-order SP-BGK scheme with two numerical integration accuracy. With the inclusion of more integration points for the numerical integral, the integration of accuracy 1 has smaller error than the integration of accuracy 2. Basically, this is a tough

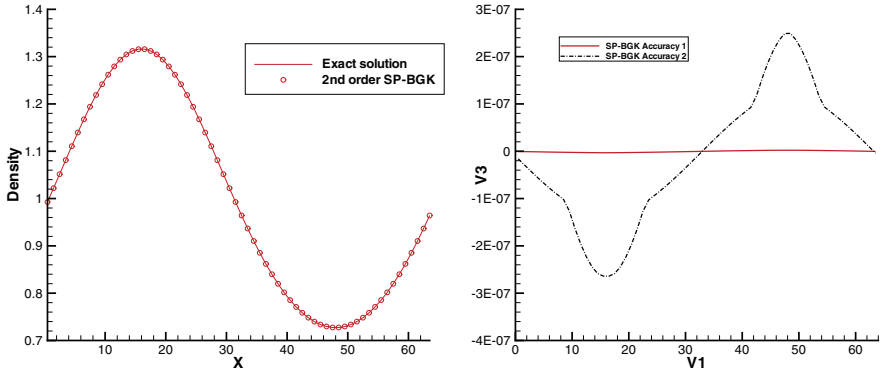

FIG. 8. *Density and temperature distributions calculated by* 2*nd-order SP-BGK for a gas falling into a fixed external potential in the* 1*-D case. The right figure shows the temperature oscillation around* 0.411958. *Accuracies* 1 *and* 2 *refer to the different accuracy for the numerical integration of the integrals. Accuracy* 1 *uses more integration points for the numerical integral and has higher accuracy than accuracy* 2.

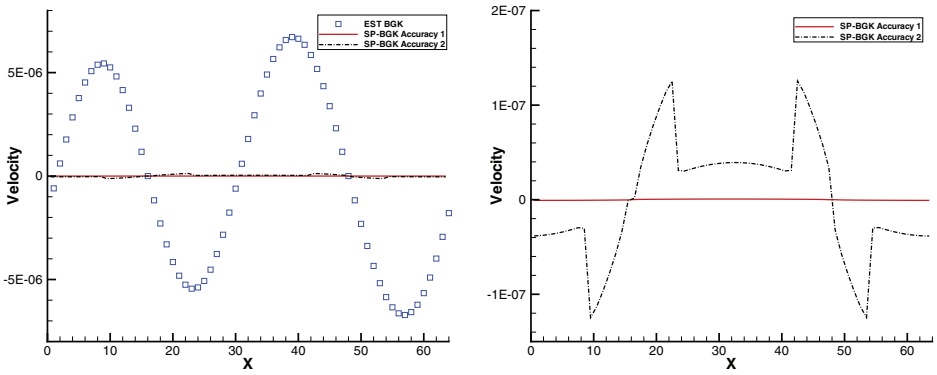

FIG. 9. *Velocity distributions for a gas falling into a fixed external potential in the* 1*-D case. The exact solution should have a zero velocity. The results from SP-BGK scheme is compared with that of the EST-BGK method* [10]. *The SP-BGK accuracy* 1 *results are closer to the exact solution. The SP-BGK scheme is a well-balanced one, where the error is due to the numerical integration of the integrals.*

test case. Due to the long time evolution, the capturing of an isothermal solution and the keeping of a constant total energy are very difficult. The results from SP-BGK scheme are the best we can find in the literature.

6.4. Rayleigh–Taylor instability. This test case also comes from [5]. Consider an isothermal equilibrium idea gas ($\gamma = 1.4$) in a 2-D polar coordinate (r, θ),

$$\rho_0(r) = e^{-\alpha(r+r_0)}, \quad p_0(r) = \frac{1.5}{\alpha} e^{-\alpha(r+r_0)}, \quad U_0 = 0,$$

where

$$\begin{cases} \alpha = 2.68,\ r_0 = 0.258 & \text{for } r \le r_1, \\ \alpha = 5.53,\ r_0 = -0.308 & \text{for } r > r_1 \end{cases} \quad \text{and} \quad \begin{cases} r_1 = 0.6(1 + 0.02\cos(20\theta)) & \text{for density}, \\ r_1 = 0.62324965 & \text{for pressure}. \end{cases}$$

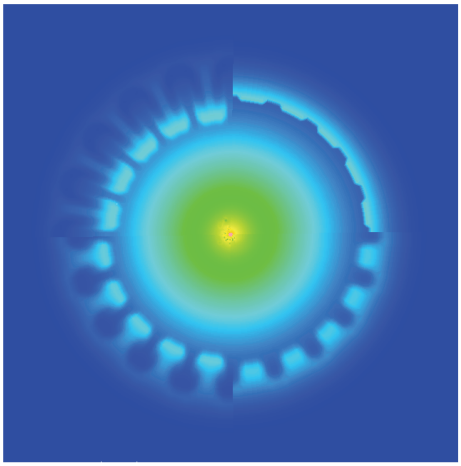

FIG. 10. *Rayleigh–Taylor instability under gravitational field directed radially inward. Density contours at time* $t = 0, 0.8, 1.4, 2.0$ *are shown in the four quadrants, starting with the initial data in the upper right corner and progressing clockwise.*

The potential satisfies $-\mathrm{d}\phi(r)/\mathrm{d}r = 1.5$. The time evolutions of the density distributions at times $t = 0$, 0.8, 1.4, and 2.0 are shown in Figure 10. Figure 11 shows a scatterplot of the density for all numerical cells as a function of the radius. These figures clearly show that the hydrostatic solution can be well kept and the flow motion is limited around the unstable interface. If a scheme is not well balanced, the solution will start to oscillate everywhere in the whole computational domain.

7. Conclusion. With the modeling of piecewise constant potential inside each cell, based on physical principles of Liouville's theorem and the symplecticity-preserving property of a Hamiltonian flow, a well-balanced gas-kinetic BGK scheme (SP-BGK) has been developed for a hydrodynamic system under gravitational field. For a hydrodynamic gravitational system, the well-balanced solution is defined as an isothermal hydrostatic solution. In order to design a well-balanced scheme, it is necessary for the equilibrium state used in the kinetic scheme to be an exact Maxwellian distribution function. At the same time, the mechanism of particle transport across a potential barrier has to follow the physical principles precisely in order to construct correct equilibrium states in the integral solution of the BGK model, and the evaluation of final fluxes. Since the physical principles for the particle transport are valid under any situation, the validity of the current scheme is not limited to the well-balanced case only. The scheme has the shock-capturing property as well for steady and unsteady flows. Mathematically, it has been proved that the SP-BGK method is a well-balanced scheme, which could keep the hydrostatic state forever after the full consideration of particle transport and collision across a potential barrier. As far as we know, this is the first method with both well-balanced and shock-capturing properties for the NS equations under gravitational field.

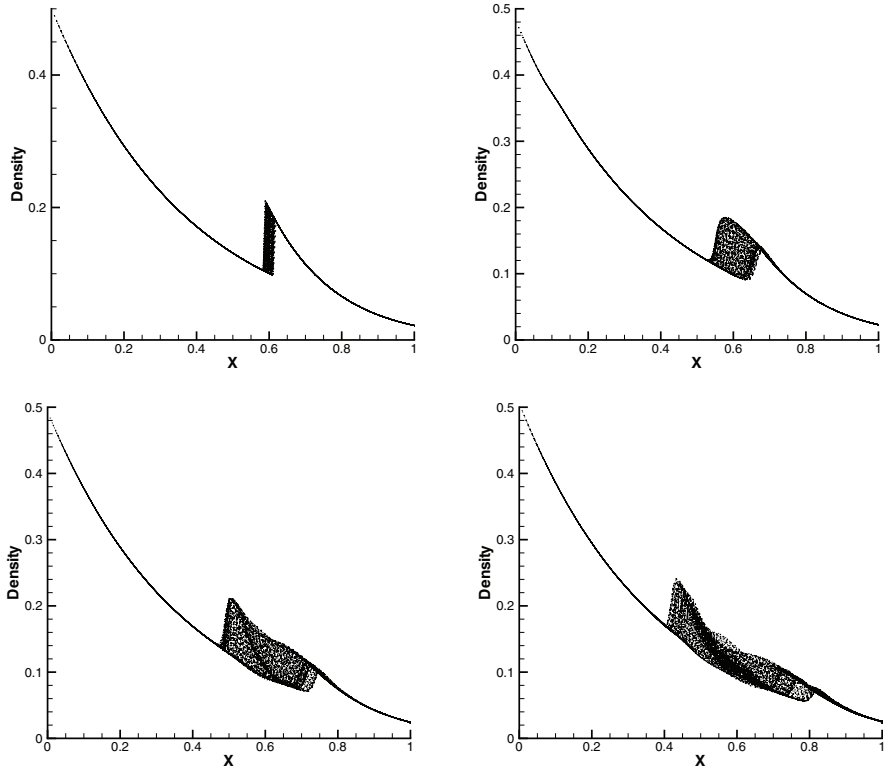

FIG. 11. *Scatterplots of the density for all cells vs. the distance of the cell center to the origin at different times. The sharp unperturbed lines demonstrate the capability of SP-BGK scheme to keep the isothermal hydrostatic solution.*

Appendix. Formulae in the 2-D case.

A.1. The construction of equilibrium states.

Case 1. $\phi_j < \phi_{j+1}$, define $U_c = \sqrt{2(\phi_{j+1} - \phi_j)}$.

(66)

$$W^l_{j+1/2} = \iiint_0^{+\infty} f_j(x_{j+1/2}, 0, u, v, \xi) \begin{pmatrix} 1 \\ u \\ v \\ \frac{1}{2}(u^2+v^2+\xi^2) \end{pmatrix} \mathrm{d}u\,\mathrm{d}v\,\mathrm{d}\xi$$

$$+ \iiint_0^{U_c} f_j(x_{j+1/2}, 0, u, v, \xi) \begin{pmatrix} 1 \\ -u \\ v \\ \frac{1}{2}(u^2+v^2+\xi^2) \end{pmatrix} \mathrm{d}u\,\mathrm{d}v\,\mathrm{d}\xi$$

$$+ \iiint_{-\infty}^0 f_{j+1}(x_{j+1/2}, 0, u, v, \xi) \begin{pmatrix} -\frac{u}{\sqrt{u^2+U_c^2}} \\ u \\ -\frac{uv}{\sqrt{u^2+U_c^2}} \\ \frac{1}{2}(-u\sqrt{u^2+U_c^2} - \frac{uv^2}{\sqrt{u^2+U_c^2}} - \frac{u}{\sqrt{u^2+U_c^2}}\xi^2) \end{pmatrix} \mathrm{d}u\,\mathrm{d}v\,\mathrm{d}\xi.$$

(67)

$$W^r_{j+1/2} = \iiint_{U_c}^{+\infty} f_j(x_{j+1/2},0,u,v,\xi) \begin{pmatrix} \frac{u}{\sqrt{u^2-U_c^2}} \\ u \\ \frac{uv}{\sqrt{u^2-U_c^2}} \\ \frac{1}{2}(u\sqrt{u^2-U_c^2}+\frac{uv^2}{\sqrt{u^2-U_c^2}}+\frac{u}{\sqrt{u^2-U_c^2}}\xi^2) \end{pmatrix} \mathrm{d}u\,\mathrm{d}v\,\mathrm{d}\xi$$
$$+ \iiint_{-\infty}^{0} f_{j+1}(x_{j+1/2},0,u,v,\xi) \begin{pmatrix} 1 \\ u \\ v \\ \frac{1}{2}(u^2+v^2+\xi^2) \end{pmatrix} \mathrm{d}u\,\mathrm{d}v\,\mathrm{d}\xi.$$

Case 2. $\phi_j > \phi_{j+1}$, define $U_c = \sqrt{2(\phi_j - \phi_{j+1})}$.

(68)

$$W^l_{j+1/2} = \iiint_{0}^{+\infty} f_j(x_{j+1/2},0,u,\xi) \begin{pmatrix} 1 \\ u \\ v \\ \frac{1}{2}(u^2+v^2+\xi^2) \end{pmatrix} \mathrm{d}u\,\mathrm{d}v\,\mathrm{d}\xi$$
$$+ \iiint_{-\infty}^{-U_c} f_{j+1}(x_{j+1/2},0,u,\xi) \begin{pmatrix} -\frac{u}{\sqrt{u^2-U_c^2}} \\ u \\ -\frac{uv}{\sqrt{u^2-U_c^2}} \\ \frac{1}{2}(-u\sqrt{u^2-U_c^2}-\frac{uv^2}{\sqrt{u^2-U_c^2}}-\frac{u}{\sqrt{u^2-U_c^2}}\xi^2) \end{pmatrix} \mathrm{d}u\,\mathrm{d}v\,\mathrm{d}\xi.$$

(69)

$$W^r_{j+1/2} = \iiint_{0}^{+\infty} f_j(x_{j+1/2},0,u,\xi) \begin{pmatrix} \frac{u}{\sqrt{u^2+U_c^2}} \\ u \\ \frac{uv}{\sqrt{u^2+U_c^2}} \\ \frac{1}{2}(u\sqrt{u^2+U_c^2}+\frac{uv^2}{\sqrt{u^2+U_c^2}}+\frac{u}{\sqrt{u^2+U_c^2}}\xi^2) \end{pmatrix} \mathrm{d}u\,\mathrm{d}v\,\mathrm{d}\xi$$
$$+ \iiint_{-U_c}^{0} f_{j+1}(x_{j+1/2},0,u,\xi) \begin{pmatrix} 1 \\ -u \\ v \\ \frac{1}{2}(u^2+v^2+\xi^2) \end{pmatrix} \mathrm{d}u\,\mathrm{d}v\,\mathrm{d}\xi$$
$$+ \iiint_{-\infty}^{0} f_{j+1}(x_{j+1/2},0,u,\xi) \begin{pmatrix} 1 \\ u \\ v \\ \frac{1}{2}(u^2+v^2+\xi^2) \end{pmatrix} \mathrm{d}u\,\mathrm{d}v\,\mathrm{d}\xi.$$

A.2. The evaluation of fluxes.
Case 1. $\phi_j < \phi_{j+1}$, define $U_c = \sqrt{2(\phi_{j+1} - \phi_j)}$.

(70)

$$F^l_{j+1/2}(t) = \iiint_0^{+\infty} f_j(x_{j+1/2}, t, u, \xi) \begin{pmatrix} u \\ u^2 \\ uv \\ \frac{1}{2}(u^3 + uv^2 + u\xi^2) \end{pmatrix} \mathrm{d}u\,\mathrm{d}v\,\mathrm{d}\xi$$
$$+ \iiint_0^{U_c} f_j(x_{j+1/2}, t, u, \xi) \begin{pmatrix} -u \\ u^2 \\ -uv \\ \frac{1}{2}(-u^3 - uv^2 - u\xi^2) \end{pmatrix} \mathrm{d}u\,\mathrm{d}v\,\mathrm{d}\xi$$
$$+ \iiint_{-\infty}^0 f_{j+1}(x_{j+1/2}, t, u, \xi) \begin{pmatrix} u \\ -u\sqrt{u^2 + U_c^2} \\ uv \\ \frac{1}{2}(u(u^2 + U_c^2) + uv^2 + u\xi^2) \end{pmatrix} \mathrm{d}u\,\mathrm{d}v\,\mathrm{d}\xi.$$

(71)

$$F^r_{j+1/2}(t) = \iiint_{U_c}^{+\infty} f_j(x_{j+1/2}, t, u, \xi) \begin{pmatrix} u \\ u\sqrt{u^2 - U_c^2} \\ uv \\ \frac{1}{2}(u(u^2 - U_c^2) + uv^2 + u\xi^2) \end{pmatrix} \mathrm{d}u\,\mathrm{d}v\,\mathrm{d}\xi$$
$$+ \iiint_{-\infty}^0 f_{j+1}(x_{j+1/2}, t, u, \xi) \begin{pmatrix} u \\ u^2 \\ uv \\ \frac{1}{2}(u^3 + uv^2 + u\xi^2) \end{pmatrix} \mathrm{d}u\,\mathrm{d}v\,\mathrm{d}\xi.$$

Case 2. $\phi_j > \phi_{j+1}$, define $U_c = \sqrt{2(\phi_j - \phi_{j+1})}$.

(72)

$$F^l_{j+1/2}(t) = \iiint_0^{+\infty} f_j(x_{j+1/2}, t, u, \xi) \begin{pmatrix} u \\ u^2 \\ uv \\ \frac{1}{2}(u^3 + uv^2 + u\xi^2) \end{pmatrix} \mathrm{d}u\,\mathrm{d}v\,\mathrm{d}\xi$$
$$+ \iiint_{-\infty}^{-U_c} f_{j+1}(x_{j+1/2}, t, u, \xi) \begin{pmatrix} u \\ -u\sqrt{u^2 - U_c^2} \\ uv \\ \frac{1}{2}(u(u^2 - U_c^2) + uv^2 + u\xi^2) \end{pmatrix} \mathrm{d}u\,\mathrm{d}v\,\mathrm{d}\xi.$$

(73)

$$F^r_{j+1/2}(t) = \iiint_0^{+\infty} f_j(x_{j+1/2},t,u,\xi)\begin{pmatrix} u \\ u\sqrt{u^2+U_c^2} \\ uv \\ \frac{1}{2}(u(u^2+U_c^2)+uv^2+u\xi^2) \end{pmatrix} \mathrm{d}u\,\mathrm{d}v\,\mathrm{d}\xi$$

$$+ \iiint_{-U_c}^0 f_{j+1}(x_{j+1/2},t,u,\xi)\begin{pmatrix} -u \\ u^2 \\ -uv \\ \frac{1}{2}(-u^3-uv^2-u\xi^2) \end{pmatrix} \mathrm{d}u\,\mathrm{d}v\,\mathrm{d}\xi$$

$$+ \iiint_{-\infty}^0 f_{j+1}(x_{j+1/2},t,u,\xi)\begin{pmatrix} u \\ u^2 \\ uv \\ \frac{1}{2}(u^3+uv^2+u\xi^2) \end{pmatrix} \mathrm{d}u\,\mathrm{d}v\,\mathrm{d}\xi.$$

Remarks on the integral evaluation. In the above formulae, there are many integrals which cannot be analytically evaluated, e.g., $\int_{-\infty}^0 f_{j+1}(-\frac{u}{\sqrt{u^2+U_c^2}})\mathrm{d}u$. Therefore, a numerical integration method as shown in [8] has been used.

REFERENCES

[1] P. L. Bhatnagar, E. P. Gross, and M. Krook, *A model for collision processes in gases* I: *Small amplitude processes in charged and neutral one-component systems*, Phys. Rev., 94 (1954), pp. 511–525.

[2] N. Botta, R. Klein, S. Langenberg, and S. Lutzenkirchen, *Well-balanced finite volume methods for nearly hydrostatic flows*, J. Comput. Phys., 196 (2004), pp. 539–565.

[3] M. J. Castro, E. D. Fernández-Nieto, A. M. Ferreiro, J. A. García-Rodríguez, and C. Parés, *High order extensions of Roe schemes for two dimensional nonconservative hyperbolic systems*, J. Sci. Comput., 39 (2009), pp. 67–114.

[4] R. J. LeVeque, *Numerical Methods for Conservation Laws*, Birkhäuser Verlag, Basel, 1992, pp. 122–135.

[5] R. J. LeVeque and D. S. Bale, *Wave propagation methods for conservation laws with source terms*, Internat. Ser. Numer. Math., 130 (1999), pp. 609–618.

[6] C. Parés and M. J. Castro, *On the well-balance property of Roe's method for nonconservative hyperbolic systems. Applications to shallow-water systems*, M2AN Math. Model. Numer. Anal., 38 (2004), pp. 821–852.

[7] B. Perthame and C. Simeoni, *A kinetic scheme for the Saint-Venant system with a source term*, CALCOLO, 38 (2001), pp. 201–231.

[8] W. H. Press, B. P. Flannery, S. A. Teukolsky, and W. T. Vetterling, *Numerical Recipes*, Cambridge University Press, Cambridge, UK, 1989.

[9] A. Slyz and K. H. Prendergast, *Time-independent gravitational fields in the BGK scheme for hydrodynamics*, Astron. Astrophys. Suppl. Ser., 139 (1999), pp. 199–217.

[10] C. L. Tian, K. Xu, K. L. Chan, and L. C. Deng, *A three-dimensional multidimensional gas kinetic scheme for the Navier-Stokes equations under gravitational fields*, J. Comput. Phys., 226 (2007), pp. 2003–2027.

[11] K. Xu, *Gas-Kinetic Schemes for Unsteady Compressible Flow Simulations*, Report 1998-03, 29th Computational Fluid Dynamics, von Karman Institute, Belgium, 1998.

[12] K. Xu, *A gas-kinetic BGK scheme for the Navier-Stokes equations, and its connection with artificial dissipation and Godunov method*, J. Comput. Phys., 171 (2001), pp. 289–335.

[13] K. Xu, J. Luo, and S. Z. Chen, *A well-balanced kinetic scheme for gas dynamic equations under gravitational field*, Adv. Appl. Math. Mech., 2 (2010), pp. 200–210.

[14] M. Zingale et al., *Mapping initial hydrostatic models in Godunov codes*, Astro. Phys. J. Suppl., 143 (2002), pp. 539–565.